




Crystal structure of danofloxacin mesylate (C<sub>19</sub>H<sub>21</sub>FN<sub>3</sub>O<sub>3</sub>)(CH<sub>3</sub>O<sub>3</sub>S)Tawnee M. Ens,<sup>1</sup> James A. Kaduk <sup>1,2,a)</sup> Anja Dosen <sup>3</sup> and Thomas N. Blanton <sup>3</sup><sup>1</sup>North Central College, 131 S. Loomis St., Naperville, IL 60540, USA<sup>2</sup>Illinois Institute of Technology, 3101 S. Dearborn St., Chicago, IL 60616, USA<sup>3</sup>ICDD, 12 Campus Blvd., Newtown Square, PA 19073-3273, USA

(Received 5 March 2023; accepted 7 July 2023)

The crystal structure of danofloxacin mesylate has been solved and refined using synchrotron X-ray powder diffraction data and optimized using density functional theory techniques. Danofloxacin mesylate crystallizes in space group *PI* (#1) with  $a = 6.77474(8)$ ,  $b = 12.4973(4)$ ,  $c = 12.82826(28)$  Å,  $\alpha = 84.8709(29)$ ,  $\beta = 87.7501(10)$ ,  $\gamma = 74.9916(4)^\circ$ ,  $V = 1044.723(11)$  Å<sup>3</sup>, and  $Z = 2$ . The protonation of the danofloxacin cations was established by the analysis of potential intermolecular interactions and differs from that expected from isolated-cation calculations. The crystal structure consists of alternating layers of cations and anions parallel to the *ac*-plane. There is parallel stacking of the oxoquinoline rings along the *a*-axis. The expected N–H...O hydrogen bonds between the cations and anions are not present. Each cation makes an N–H...O hydrogen bond with the other cation, resulting in zig-zag chains along the *a*-axis. Both cations have strong intramolecular O–H...O hydrogen bonds. There are several C–H...O hydrogen bonds between the danofloxacin cations and mesylate anions. The powder pattern has been submitted to ICDD® for inclusion in the Powder Diffraction File™ (PDF®).

© The Author(s), 2023. Published by Cambridge University Press on behalf of International Centre for Diffraction Data. This is an Open Access article, distributed under the terms of the Creative Commons Attribution licence (<http://creativecommons.org/licenses/by/4.0/>), which permits unrestricted re-use, distribution and reproduction, provided the original article is properly cited.

[doi:10.1017/S0885715623000271]

Key words: danofloxacin mesylate, advocin®, crystal structure, Rietveld refinement, density functional theory

## I. INTRODUCTION

Danofloxacin mesylate (sold under the brand name Advocin) is an antibiotic, used to treat respiratory disease in cattle (Halleran et al., 2021), that belongs to the fluoroquinolone class of veterinary antibiotics approved for use in the US by the FDA (2023). Danofloxacin in humans can cause minor eye, skin, and gastrointestinal irritation, as well as gastrointestinal irritation in animals, and is not approved for human use by the FDA (2022). Danofloxacin mesylate is rapidly distributed and found in high levels in the mammary glands, and respiratory and intestinal tracts following subcutaneous, intramuscular, or intravenous injection in livestock animals (Schrickx and Fink-Gremmels, 2007). The metabolites found after administration included N-desmethyl- and unmetabolized danofloxacin, and NO. The European Medicines Agency (EMA) found very high doses, around 100–200 mg/kg body weight/day, also caused toxic fetal and maternal effects in rats and mice (1997).

The systematic name (CAS Registry Number 119478-55-6) is 1-cyclopropyl-6-fluoro-7-[(1*S*,4*S*)-5-methyl-2,5-diazabicyclo[2.2.1]heptan-2-yl]-4-oxoquinoline-3-carboxylic acid methane-sulfonate. A two-dimensional molecular diagram is shown in

Figure 1. We are unaware of any published X-ray powder diffraction data on danofloxacin mesylate.

This work was carried out as part of a project (Kaduk et al., 2014) to determine the crystal structures of large-volume commercial pharmaceuticals and include high-quality powder diffraction data for them in the Powder Diffraction File (Gates-Rector and Blanton, 2019).

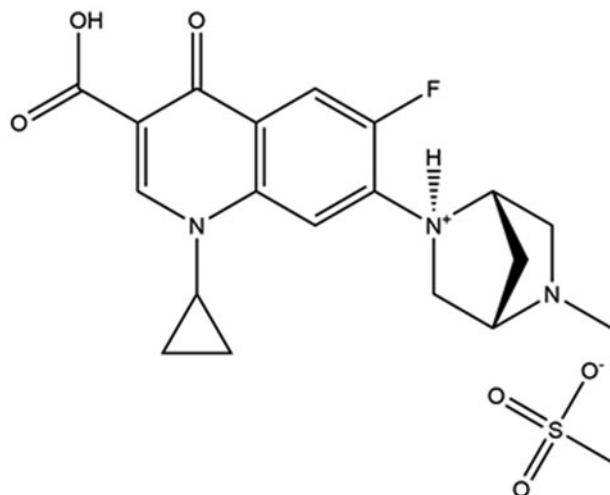


Figure 1. The 2D molecular structure of danofloxacin mesylate.

<sup>a)</sup> Author to whom correspondence should be addressed. Electronic mail: [kaduk@polycrystallography.com](mailto:kaduk@polycrystallography.com)

## II. EXPERIMENTAL

Danofloxacin mesylate was a commercial reagent, purchased from TargetMol (Batch #115470), and was used as-received. The white powder was packed into a 1.5 mm diameter Kapton capillary and rotated during the measurement at ~50 Hz. The powder pattern was measured at 295 K at beamline 11-BM (Antao et al., 2008; Lee et al., 2008; Wang et al., 2008) of the Advanced Photon Source at Argonne National Laboratory using a wavelength of 0.458208(2) Å from 0.5 to 50° 2θ with a step size of 0.001° and a counting time of 0.1 s/step. The high-resolution powder diffraction data were collected using 12 silicon crystal analyzers that allow for high angular resolution, high precision, and accurate peak positions. A mixture of silicon (NIST SRM 640c) and alumina (NIST SRM 676a) standards (ratio Al<sub>2</sub>O<sub>3</sub>:Si = 2:1 by weight) was used to calibrate the instrument and refine the monochromatic wavelength used in the experiment.

The pattern was indexed using N-TREOR (Altomare et al., 2013) on a primitive triclinic unit cell with  $a = 6.77464$ ,  $b = 12.49476$ ,  $c = 12.83040$  Å,  $\alpha = 84.879$ ,  $\beta = 87.734$ ,  $\gamma = 75.046^\circ$ ,  $V = 1044.9$  Å<sup>3</sup>, and  $Z = 2$ . A reduced cell search in the Cambridge Structural Database (Groom et al., 2016) yielded no hits. Since danofloxacin is a chiral molecule, we assumed the space group for danofloxacin mesylate to be *P1*, resulting in two cations and two anions in the asymmetric unit. Structure solutions in space group *P1* yielded significantly higher residuals.

The danofloxacin molecule was downloaded from PubChem (Kim et al., 2023) as Conformer3D\_CID\_71335.sdf, and converted to a \*.mol2 file using Mercury (Macrae et al., 2020). The mesylate anion was built using *Spartan* '18 (Wavefunction, 2020), and saved as a \*.mol2 file. The crystal structure was solved using Monte Carlo simulated annealing techniques as implemented in DASH (David et al., 2006), including Mogul Distribution Bias.

Many solutions were examined visually, and the 11 best solutions were refined. Among the solutions, there were variations in the orientation of the cyclopropane rings and the methyl group on the diazabicycloheptane cage. In the two best solutions, the orientations of these groups were the same. Among the solutions, there were also variations in the orientations of the mesylate anions. This might not be surprising, as the mesylate consists of a tetrahedral S atom surrounded by three O atoms and a methyl group. It may be difficult to distinguish 8 (O) from 9 (CH<sub>3</sub>) electrons using X-ray powder data. In the two best solutions the orientation of one of the mesylates was the same, while the other differed; the methyl group and one of the O atoms were interchanged. We attempted a refinement of a disordered model, but it was unstable and yielded chemically unreasonable results. Since we need an ordered model to perform DFT calculations, we concentrated on ordered models, though there may be some disorder of both the mesylate anions and the danofloxacin cations.

An additional feature of the structure solution is identifying which of the three N atoms of each cation is protonated. Normally, this is straightforward, as a short N–H...O hydrogen bond between the cation and anion can be identified. This was not the case in this structure.

Two different protonated states of danofloxacin have been identified (McCullagh et al., 2018). Danofloxacin protomer I

is protonated on the keto group of the oxoquinoline ring system. Protomer II is protonated at either what was designated as N6 or N5 (slightly less favorable). Each N atom is prochiral; protonating on the “up” or “down” sides yields another chiral center, so we had to consider protonating on either side of each N atom. Spartan calculations of isolated cations (DFT/B3LYP/6-31G\*/water) suggested that protonation at N6 was most favorable. Cations protonated at N5 were 19 kcal/mol higher in energy (as suggested by McCullagh et al.), and those protonated at N7 were 53 kcal/mol higher in energy.

In the solid state, there are no particularly close N...O distances, so the normal/expected hydrogen bonds are not apparent. For N6 (and N52), the shortest N...O distance is >4.00 Å. For N7 (and N53), the shortest distances are 3.34 and 3.45 Å. For N5 (and N51), the shortest distances are 2.79/3.17 and 2.91 Å – both to O50/O49 and O3 of the carboxylic acid groups. Among these O atoms, the hydroxyl group is the most negative (from the isolated cation calculations), so it is not an unreasonable place for a long N–H...O hydrogen bond and seems to be the most likely acceptor for the proton. The next shortest N...O distances are to the carbonyl groups of the carboxylic acids, in the “other” directions. The expected N–H...O hydrogen bonds between the cations and mesylate anions are not present. Positions of H109 and H110 were derived by placing them on the shortest N...O vectors.

Rietveld refinement was carried out using GSAS-II (Toby and Von Dreele, 2013). Only the 2.0–25.0° portion of the pattern was included in the refinement ( $d_{\min} = 1.058$  Å). All non-H bond distances and angles were subjected to restraints, based on a Mercury/Mogul Geometry check (Bruno et al., 2004; Sykes et al., 2011). The Mogul average and standard deviation for each quantity were used as the restraint parameters. The restraints contributed 12.0% to the final  $\chi^2$ . The hydrogen atoms were included in calculated positions, which were recalculated during the refinement using Materials Studio (Dassault Systèmes, 2021). The  $U_{iso}$  of the heavy atoms were grouped by chemical similarity. The  $U_{iso}$  for the H atoms were fixed at 1.3× the  $U_{iso}$  of the heavy atoms to which they are attached. No preferred orientation model was included in the refinement. The peak profiles were described using the generalized microstrain model (Stephens, 1999). The background was modeled using a 3-term shifted Chebyshev polynomial, and a peak at 7.31° 2θ to model the scattering from the Kapton capillary and any amorphous component.

The final refinement (begun from the DFT-optimized structure) of 216 variables using 23,037 observations and 180 restraints yielded the residuals  $R_{wp} = 0.1089$  and  $GOF = 2.27$ . The largest peak (0.91 Å from O50) and hole (1.76 Å from C55) in the difference Fourier map were 0.55(12) and  $-0.50(12)$  eÅ<sup>-3</sup>, respectively. The largest errors in the difference plot (Figure 2) are in the intensities of some of the peaks and may reflect the simplified model used here.

The structure of danofloxacin mesylate was optimized (fixed experimental unit cell) with density functional techniques using VASP (Kresse and Furthmüller, 1996) through the MedeA graphical interface (Materials Design, 2016). The calculation was carried out on 16 2.4 GHz processors (each with 4 Gb RAM) of a 64-processor HP Proliant DL580 Generation 7 Linux cluster at North Central College. The calculation used the GGA-PBE functional, a plane wave cutoff energy of 400.0 eV, and a *k*-point spacing of

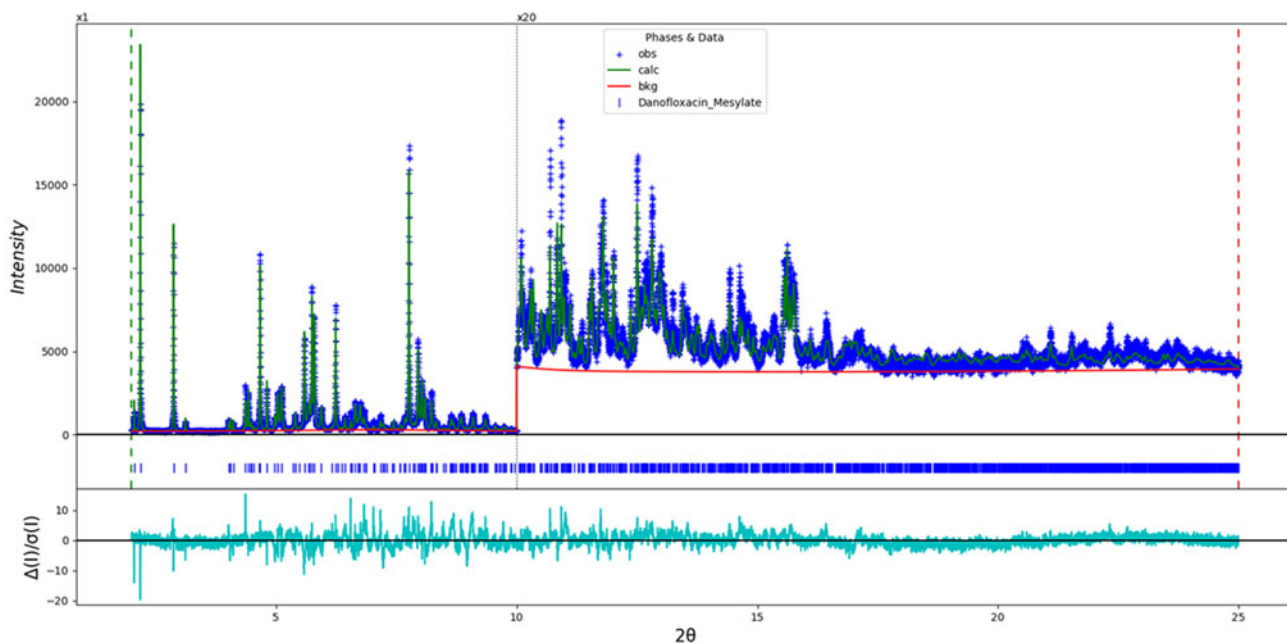


Figure 2. The Rietveld plot for the refinement of danofloxacin mesylate. The blue crosses represent the observed data points, and the green line is the calculated pattern. The cyan curve is the normalized error plot, and the red line is the background curve. The vertical scale has been multiplied by a factor of 20× for  $2\theta > 10.0^\circ$ .

$0.5 \text{ \AA}^{-1}$  leading to a  $2 \times 2 \times 1$  mesh, and took  $\sim 13$  h. Single-point density functional theory calculations (fixed experimental cell) and population analysis were carried out using CRYSTAL23 (Erba et al., 2023). The basis sets for the H, C, N, and O atoms in the calculation were those of Gatti et al. (1994), and those for F and S were those of Peintinger et al. (2013). The calculations were run on a 3.5 GHz PC using 8  $k$ -points and the B3LYP functional and took  $\sim 6.4$  h.

### III. RESULTS AND DISCUSSION

The strong N–H $\cdots$ O hydrogen bonds which might have been expected between the cations and the anions are not present. Although calculations of isolated cations suggest that the protonation of N6 yields the lowest-energy structure, the solid-state interactions indicate that N5 is protonated in both cations.

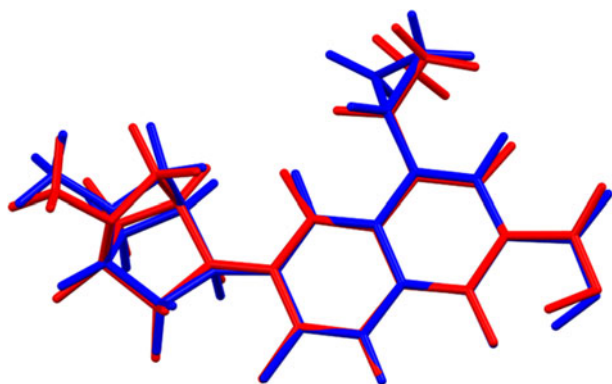


Figure 3. Comparison of the Rietveld-refined (red) and VASP-optimized (blue) structures of danofloxacin cation 1. The rms Cartesian displacement is  $0.353 \text{ \AA}$ . Image generated using Mercury (Macrae et al., 2020).

The root-mean-square Cartesian displacement between the Rietveld-refined and DFT-optimized structures of cation 1 (the lower atom numbers) is  $0.353 \text{ \AA}$  (Figure 3). The similar quantity for the cation 2 is  $0.266 \text{ \AA}$  (Figure 4). The agreements are within the normal range for correct structures (van de Streek and Neumann, 2014), and provide evidence that the refined structure is correct. The greatest differences are in the methyl groups on the diazabicycloheptane cages, and may indicate that protonation at N5 is not completely uniform; protonation on the “up” or “down” side of N5 results in a significant difference in the cage conformation. This discussion concentrates on the VASP-optimized structure. The rms difference between cation 1 and cation 2 is  $1.209 \text{ \AA}$  (Figure 5). The major differences are in the orientations of the diazabicycloheptane cages; they differ in orientation by approximately  $180^\circ$ . The asymmetric unit (with atom numbering) is illustrated in Figure 6.

The crystal structure consists of alternating layers of cations and anions parallel to the  $ac$ -plane (Figure 7). There is parallel stacking of the oxoquinoline rings along the  $a$ -axis.

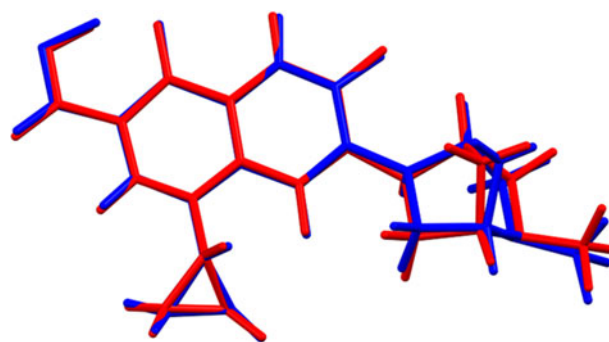


Figure 4. Comparison of the Rietveld-refined (red) and VASP-optimized (blue) structures of danofloxacin cation 2. The rms Cartesian displacement is  $0.266 \text{ \AA}$ . Image generated using Mercury (Macrae et al., 2020).

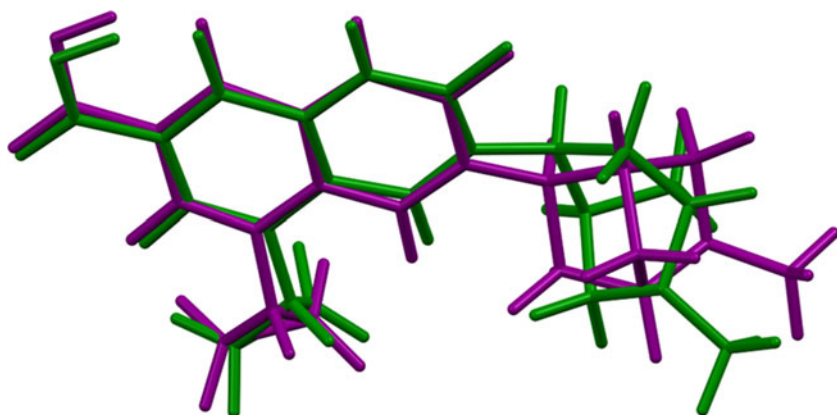


Figure 5. Comparison of the structure of danofloxacin cation 1 (green) and cation 2 (purple). The rms Cartesian displacement is 1.209 Å. Image generated using Mercury (Macrae et al., 2020).

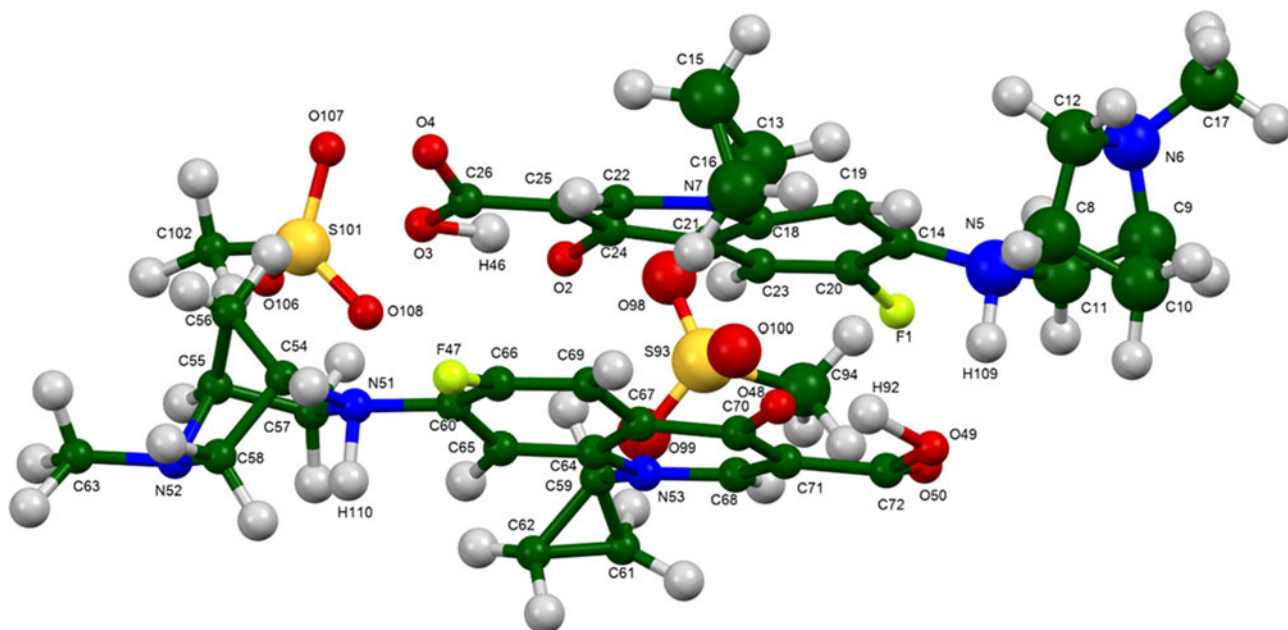


Figure 6. The asymmetric unit of danofloxacin mesylate, with the atom numbering. The atoms are represented by 50% probability spheroids. Image generated using Mercury (Macrae et al., 2020).

The mean planes of the oxoquinoline rings are (11,6,2) for cation 1 and (12,6,−1) for cation 2. The Mercury Aromatics Analyser indicates one moderate interaction of 5.34 Å between the two cations. N–H⋯O hydrogen bonds link the cations into zig-zag chains along the *a*-axis.

All of the bond distances and bond angles fall within the normal ranges indicated by a Mercury Mogul Geometry check (Macrae et al., 2020). Torsion angles involving rotation about the C13–N7 (and C59–N53) bonds lie on the tails of bimodal distributions and are flagged as unusual. Torsion angles involving rotation about the C14–N5 (and C60–N51) bonds yielded either few or no hits. These reflect the orientation of the cage and oxoquinoline fragments at the protonated nitrogens and indicate that these danofloxacin cations are truly unusual.

Quantum chemical geometry optimization of the isolated cations (DFT/B3LYP/6-31G\*/water) using Spartan '18 (Wavefunction, 2020) indicated that cation 2 is lower in energy than cation 1 by 2.5 kcal/mol. The global minimum-energy conformation (MMFF force field) is 5.4 kcal/mol lower in energy and has a very different conformation. The

molecule curls up on itself to bring N6 and the carboxylic acid group close together. Thus intermolecular interactions are important to determining the solid-state conformation.

Analysis of the contributions to the total crystal energy of the structure using the Forcite module of Materials Studio (Dassault Systèmes, 2021) suggests that angle distortion terms dominate the intramolecular deformation energy. The intermolecular energy is dominated by electrostatic attractions, which in this force field analysis also include hydrogen bonds. The hydrogen bonds are better analyzed using the results of the DFT calculation.

The expected N–H⋯O hydrogen bonds between the cations and anions are not present (Table I). Each cation does make an N–H⋯O hydrogen bond to the other cation. The acceptors O50 and O3 in the carboxylic acid groups are more negative than the O atoms in the mesylate anions, so are reasonable acceptors in hydrogen bonds. The charges of these O atoms differ by the most between the two cations. The N–H⋯O hydrogen bonds link the cations in zig-zag chains along the *a*-axis, with a graph set (Etter, 1990; Bernstein et al., 1995; Shields et al., 2000) of  $C2,2(20)$ . The

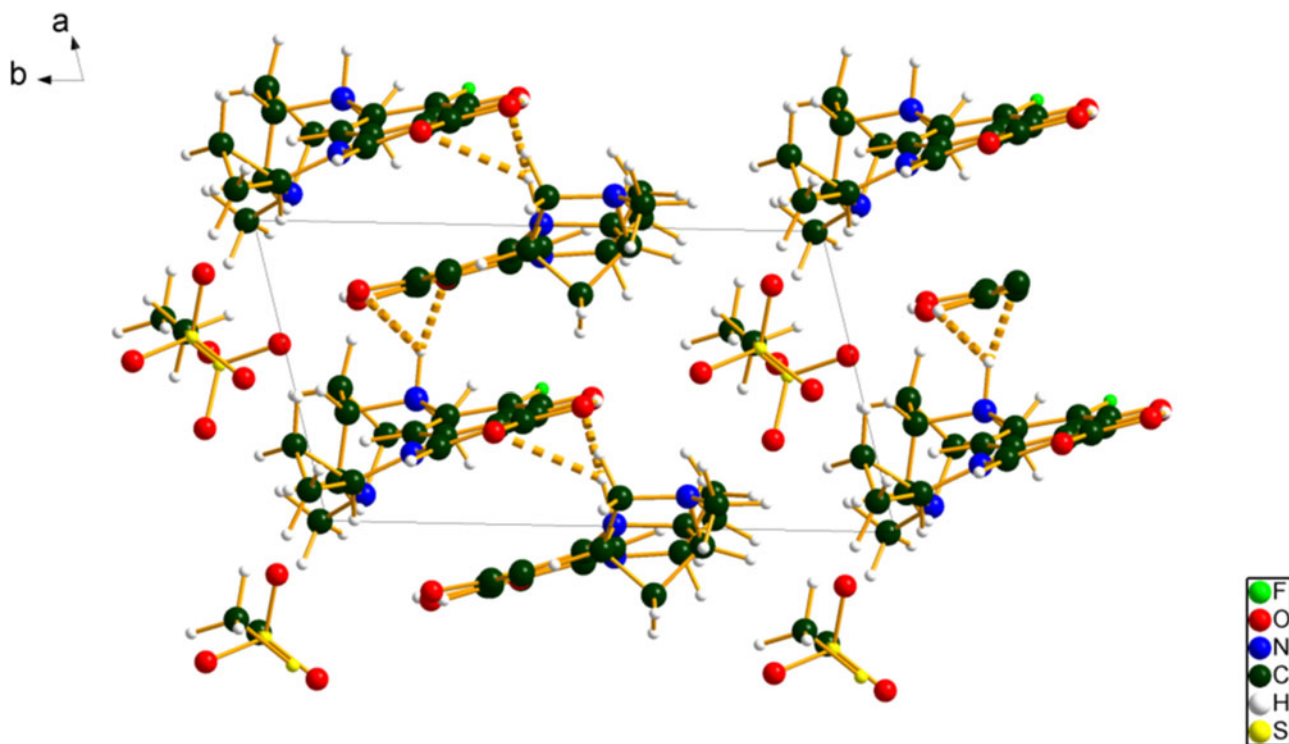


Figure 7. The crystal structure of danofloxacin mesylate, viewed down the *c*-axis. Image generated using Diamond (Crystal Impact, 2022).

TABLE I. Hydrogen bonds (CRYSTAL23) in danofloxacin mesylate.

H-Bond	D–H, Å	H...A, Å	D...A, Å	D–H...A, <sup>a</sup>	Overlap, <i>e</i>	<i>E</i> , kcal/mol
N5–H109...O50	1.061	1.789	2.789	155.4	0.073	6.2
N51–H110...O3	1.046	1.977	2.910	147.0	0.039	4.6
O3–H46...O2	1.086	1.403 <sup>a</sup>	2.445	158.1	0.116	18.6
O49–H92...O48	1.051	1.511 <sup>a</sup>	2.491	152.6	0.088	16.2
C8–H27...O98	1.098	2.334	3.376	157.8	0.033	
C9–H28...O4	1.092	2.401	3.166	125.7	0.015	
C57–H77...O107	1.099	2.143	3.085	142.2	0.041	
C12–H33...O49	1.100	2.597	3.634	156.8	0.010	
C58–H80...O50	1.102	2.676	3.495	137.1	0.012	
C13–H35...O48	1.092	2.425	3.181	125.1	0.009	
C59–H81...O2	1.093	2.482	3.369	137.5	0.013	
C15–H37...O108	1.092	2.620	3.644	155.8	0.019	
C61–H83...O99	1.092	2.590	3.672	170.6	0.018	
C16–H38...O98	1.086	2.403	3.048	116.6	0.010	
C62–H84...O107	1.088	2.597	3.376	127.9	0.011	
C16–H39...O48	1.089	2.622	3.514	138.6	0.008	
C16–H39...O108	1.089	2.640	3.277	116.7	0.008	
C62–H85...O2	1.090	2.493	3.495	152.4	0.012	
C17–H41...O107	1.111	2.741	3.773	154.3	0.012	
C63–H88...O100	1.098	2.374	3.444	164.2	0.030	
C17–H42...O106	1.099	2.724	3.524	129.3	0.011	
C19–H43...C13	1.090	2.469 <sup>a</sup>	2.829	97.7	0.010	
C65–H89...C59	1.088	2.442 <sup>a</sup>	2.829	99.3	0.014	
C22–H44...O4	1.089	2.586 <sup>a</sup>	2.873	93.8	0.011	
C68–H90...O50	1.090	2.558 <sup>a</sup>	2.848	93.9	0.010	
C23–H45...O2	1.094	2.545 <sup>a</sup>	2.832	93.5	0.008	
C69–H91...O48	1.096	2.568 <sup>a</sup>			0.009	
C69–H91...O106	1.096	2.737	3.695	110.0	0.018	
C94–H95...N52	1.097	2.706	3.767	162.6	0.016	

Top, molecule 1; bottom, molecule 2.

<sup>a</sup>Intramolecular.

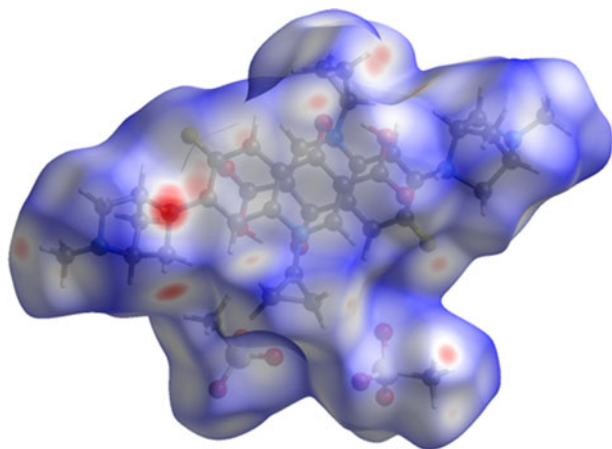


Figure 8. The Hirshfeld surface of danofloxacin mesylate. Intermolecular contacts longer than the sums of the van der Waals radii are colored blue, and contacts shorter than the sums of the radii are colored red. Contacts equal to the sums of radii are white. Image generated using CrystalExplorer (Spackman et al., 2021).

energies of the N–H...O hydrogen bonds were calculated using the correlation of Wheatley and Kaduk (2019).

Both cations have strong intramolecular O–H...O hydrogen bonds, as expected from the relative orientation of the carbonyl and carboxylic acid groups. The energies of the O–H...O hydrogen bonds were calculated using the correlation of Rammohan and Kaduk (2018). Each diazabicycloheptane cage makes a strong (judged by the Mulliken overlap population) C–H...O hydrogen bond to a mesylate anion. In one cation the donor is a methyne group and in the other, it is a methylene group. This is one of a number of subtle differences in the interactions of the two cations. There are a variety of other C–H...O hydrogen bonds, both to mesylates and O atoms of the cations. There is a C94–H95...N52 hydrogen bond from a mesylate anion to an N atom in a cation cage. Both cyclopropyl bridgehead carbon atoms C13 and C59 act as an acceptor in an intramolecular C–H...C hydrogen bond.

The volume enclosed by the Hirshfeld surface of the danofloxacin mesylate asymmetric unit (Figure 8, Hirshfeld, 1977; Spackman et al., 2021) is 1034.25 Å<sup>3</sup>, 99.00% of the unit cell volume. The packing density is thus fairly typical. The only significant close contacts (red in Figure 8) involve the hydrogen bonds. The volume per non-hydrogen atom is smaller than normal, at 16.8 Å<sup>3</sup>.

The Bravais–Friedel–Donnay–Harker (Bravais, 1866; Friedel, 1907; Donnay and Harker, 1937) morphology suggests that we might expect elongated morphology for danofloxacin mesylate, with <100> as the long axis. No preferred orientation model was necessary, indicating that preferred orientation was not present in this rotated capillary specimen.

#### IV. DEPOSITED DATA

The powder pattern of danofloxacin mesylate from this synchrotron data set has been submitted to ICDD for inclusion in the Powder Diffraction File. The Crystallographic Information Framework (CIF) files containing the results of the Rietveld refinement (including the raw data) and the DFT geometry optimization were deposited with the ICDD. The data can be requested at [pdj@icdd.com](mailto:pdj@icdd.com).

#### ACKNOWLEDGEMENTS

Use of the Advanced Photon Source at Argonne National Laboratory was supported by the U. S. Department of Energy, Office of Science, Office of Basic Energy Sciences, under Contract No. DE-AC02-06CH11357. This work was partially supported by the International Centre for Diffraction Data. We thank Lynn Ribaud and Saul Lapidus for their assistance in the data collection.

#### CONFLICTS OF INTEREST

The authors have no conflicts of interest to declare.

#### REFERENCES

- Altomare, A., C. Cuocci, C. Giacovazzo, A. Moliterni, R. Rizzi, N. Corriero, and A. Falcicchio. 2013. "EXPO2013: a Kit of Tools for Phasing Crystal Structures from Powder Data." *Journal of Applied Crystallography* 46: 1231–1235.
- Antao, S. M., I. Hassan, J. Wang, P. L. Lee, and B. H. Toby. 2008. "State-of-the-Art High-Resolution Powder X-Ray Diffraction (HRPXR) Illustrated with Rietveld Refinement of Quartz, Sodalite, Tremolite, and Meionite." *Canadian Mineralogist* 46: 1501–1509.
- Bernstein, J., R. E. Davis, L. Shimoni, and N. L. Chang. 1995. "Patterns in Hydrogen Bonding: Functionality and Graph Set Analysis in Crystals." *Angewandte Chemie International Edition in English* 34: 1555–1573.
- Bravais, A. 1866. *Etudes Cristallographiques*. Paris, Gauthier Villars.
- Bruno, I. J., J. C. Cole, M. Kessler, J. Luo, W. D. S. Motherwell, L. H. Purkis, B. R. Smith, R. Taylor, R. I. Cooper, S. E. Harris, and A. G. Orpen. 2004. "Retrieval of Crystallographically-Derived Molecular Geometry Information." *Journal of Chemical Information and Computer Sciences* 44: 2133–2144.
- Center for Veterinary Medicine, Food and Drug Administration, U.S. Department of Health and Human Services. 2022. "Extralabel Use and Antimicrobials". <https://www.fda.gov/animal-veterinary/antimicrobial-resistance/extralabel-use-and-antimicrobials>.
- Center for Veterinary Medicine, Food and Drug Administration, U.S. Department of Health and Human Services. 2023. "Evaluating the Safety of Antimicrobial New Animal Drugs with Regard to their Microbiological Effects on Bacteria of Human Health Concern; Guidance for Industry; Draft Guidance". <https://www.fda.gov/media/69949/download>.
- Crystal Impact. 2022. Diamond. V. 4.6.8. Crystal Impact – Dr. H. Putz & Dr. K. Brandenburg. Windows.
- Dassault Systèmes. 2021. *Materials Studio 2021*. San Diego, CA, BIOVIA.
- David, W. I. F., K. Shankland, J. van de Streek, E. Pidcock, W. D. S. Motherwell, and J. C. Cole. 2006. "DASH: A Program for Crystal Structure Determination from Powder Diffraction Data." *Journal of Applied Crystallography* 39: 910–915.
- Donnay, J. D. H., and D. Harker. 1937. "A New Law of Crystal Morphology Extending the Law of Bravais." *American Mineralogist* 22: 446–447.
- Erba, A., J. K. Desmaris, S. Casassa, B. Civalieri, L. Donà, I. J. Bush, B. Searle, L. Maschio, L.-E. Daga, A. Cossard, C. Ribaldone, E. Ascrizzi, N. L. Marana, J.-P. Flament, and B. Kirtman. 2023. "CRYSTAL23: A Program for Computational Solid State Physics and Chemistry." *Journal of Chemical Theory and Computation*. doi:10.1021/acs.jctc.2c00958.
- Etter, M. C. 1990. "Encoding and Decoding Hydrogen-Bond Patterns of Organic Compounds." *Accounts of Chemical Research* 23: 120–126.
- Friedel, G. 1907. "Etudes sur la loi de Bravais." *Bulletin de la Société Française de Minéralogie* 30: 326–455.
- Gates-Rector, S., and T. N. Blanton. 2019. "The Powder Diffraction File: A Quality Materials Characterization Database." *Powder Diffraction* 39: 352–360.
- Gatti, C., V. R. Saunders, and C. Roetti. 1994. "Crystal-Field Effects on the Topological Properties of the Electron-Density in Molecular Crystals – The Case of Urea." *Journal of Chemical Physics* 101: 10686–10696.

- Groom, C. R., I. J. Bruno, M. P. Lightfoot, and S. C. Ward. 2016. "The Cambridge Structural Database." *Acta Crystallographica Section B: Structural Science, Crystal Engineering and Materials* 72: 171–179.
- Halleran, J. L., B. J. Callahan, M. E. Jacob, H. J. Sylvester, T. Prange, M. G. Papich, and D. M. Foster. 2021. "Effects of Danofloxacin Dosing Regimen on Gastrointestinal Pharmacokinetics and Fecal Microbiome in Steers." *Scientific Reports* 11: 11249.
- Hirshfeld, F. L. 1977. "Bonded-Atom Fragments for Describing Molecular Charge Densities." *Theoretica Chimica Acta* 44: 129–138.
- Kaduk, J. A., C. E. Crowder, K. Zhong, T. G. Fawcett, and M. R. Suchomel. 2014. "Crystal Structure of Atomoxetine Hydrochloride (Strattera), C<sub>17</sub>H<sub>22</sub>NOCl." *Powder Diffraction* 29: 269–273.
- Kim, S., J. Chen, T. Cheng, A. Gindulyte, J. He, S. He, Q. Li, B. A. Shoemaker, P. A. Thiessen, B. Yu, L. Zaslavsky, J. Zhang, and E. E. Bolton. 2023. "Pubchem 2023 Update." *Nucleic Acids Research* 51 (D1): D1373–D1380. doi:10.1093/nar/gkac956.
- Kresse, G., and J. Furthmüller. 1996. "Efficiency of Ab-Initio Total Energy Calculations for Metals and Semiconductors Using a Plane-Wave Basis Set." *Computational Materials Science* 6: 15–50.
- Lee, P. L., D. Shu, M. Ramanathan, C. Preissner, J. Wang, M. A. Beno, R. B. Von Dreele, L. Ribaud, C. Kurtz, S. M. Antao, X. Jiao, and B. H. Toby. 2008. "A Twelve-Analyzer Detector System for High-Resolution Powder Diffraction." *Journal of Synchrotron Radiation* 15: 427–432.
- Macrae, C. F., I. Sovago, S. J. Cottrell, P. T. A. Galek, P. McCabe, E. Pidcock, M. Platings, G. P. Shields, J. S. Stevens, M. Towler, and P. A. Wood. 2020. "Mercury 4.0: From Visualization to Design and Prediction." *Journal of Applied Crystallography* 53: 226–235.
- Materials Design. 2016. *MedeA 2.20.4*. Angel Fire, NM, Materials Design Inc.
- McCullagh, M., K. Giles, K. Richardson, S. Stead, and M. Palmer. 2018. "Investigations into the Performance of Travelling Wave Enabled Conventional and Cyclic Ion Mobility Systems to Characterise Protomers of Fluoroquinolone Antibiotic Residues." *Rapid Communications in Mass Spectrometry* 2019: 1–11.
- Peintinger, M. F., D. Vilela Oliveira, and T. Bredow. 2013. "Consistent Gaussian Basis Sets of Triple-Zeta Valence with Polarization Quality for Solid-State Calculations." *Journal of Computational Chemistry* 34: 451–459.
- Rammohan, A., and J. A. Kaduk. 2018. "Crystal Structures of Alkali Metal (Group 1) Citrate Salts." *Acta Crystallographica Section B: Crystal Engineering and Materials* 74: 239–252. doi:10.1107/S2052520618002330.
- Schrickx, J. A., and J. Fink-Gremmels. 2007. "Danofloxacin Mesylate is a Substrate for ATP Dependent Efflux Transporters." *British Journal of Pharmacology* 150: 463–469.
- Shields, G. P., P. R. Raithby, F. H. Allen, and W. D. S. Motherwell. 2000. "The Assignment and Validation of Metal Oxidation States in the Cambridge Structural Database." *Acta Crystallographica Section B: Structural Science* 56: 455–465.
- Spackman, P. R., M. J. Turner, J. J. McKinnon, S. K. Wolff, D. J. Grimwood, D. Jayatilaka, and M. A. Spackman. 2021. "Crystalexplorer: A Program for Hirshfeld Surface Analysis, Visualization and Quantitative Analysis of Molecular Crystals." *Journal of Applied Crystallography* 54: 1006–1011. doi:10.1107/S1600576721002910
- Stephens, P. W. 1999. "Phenomenological Model of Anisotropic Peak Broadening in Powder Diffraction." *Journal of Applied Crystallography* 32: 281–289.
- Sykes, R. A., P. McCabe, F. H. Allen, G. M. Battle, I. J. Bruno, and P. A. Wood. 2011. "New Software for Statistical Analysis of Cambridge Structural Database Data." *Journal of Applied Crystallography* 44: 882–886.
- The European Agency for the Evaluation of Medicinal Products, Veterinary Medicines Evaluation Unit, Committee for Veterinary Medicinal Products. 1997. "Danofloxacin Summary Report (2)." [https://www.ema.europa.eu/en/documents/mrl-report/danofloxacin-summary-report-2-committee-veterinary-medicinal-products\\_en.pdf](https://www.ema.europa.eu/en/documents/mrl-report/danofloxacin-summary-report-2-committee-veterinary-medicinal-products_en.pdf).
- Toby, B. H., and R. B. Von Dreele. 2013. "GSAS II: The Genesis of a Modern Open Source All Purpose Crystallography Software Package." *Journal of Applied Crystallography* 46: 544–549.
- van de Streek, J., and M. A. Neumann. 2014. "Validation of Molecular Crystal Structures from Powder Diffraction Data with Dispersion-Corrected Density Functional Theory (DFT-D)." *Acta Crystallographica Section B: Structural Science, Crystal Engineering and Materials* 70: 1020–1032.
- Wang, J., B. H. Toby, P. L. Lee, L. Ribaud, S. M. Antao, C. Kurtz, M. Ramanathan, R. B. Von Dreele, and M. A. Beno. 2008. "A Dedicated Powder Diffraction Beamline at the Advanced Photon Source: Commissioning and Early Operational Results." *Review of Scientific Instruments* 79: 085105.
- Wavefunction, Inc. 2020. Spartan '18. Version 1.4.5. Wavefunction Inc., 18401 Von Karman Ave., Suite 370, Irvine CA 96212.
- Wheatley, A. M., and J. A. Kaduk. 2019. "Crystal Structures of Ammonium Citrates." *Powder Diffraction* 34: 35–43.